OPEN ACCESS Freely available online

AFM Applied Functional Materials

ISSN 2737-5323
Volume 6
Issue 2
Applied Functional Materials

Article

Properties of the Horizontal Structural P-Type β-Ga_2O_3 Schottky Barrier Diode Fabricated by the Thermal Oxidation of GaN in N_2O Environment

Hangcheng Zhou [1], Xinping Wang [2], Weijun Chen [3] and Sufen Wei [1,*]

[1] School of Ocean Information Engineering, Jimei University, Xiamen 361021, China; zhc1999@139.com
[2] School of Science, Jimei University, Xiamen 361021, China; 15580249348@139.com
[3] School of Electronic Science and Technology, Xiamen University, Xiamen 361005, China; 36620231150388@stu.xmu.edu.cn
* Correspondence: weisufen@jmu.edu.cn

Received: Jul 21, 2025; **Revised:** Sep 12, 2025; **Accepted:** Dec 20, 2025; **Published:** Jun 30, 2026

Abstract: Schottky barrier diodes (SBDs) are high-speed, low-power electronic devices that are widely used in high-frequency and microwave communication circuits, as well as in power electronics. In this study, thermal oxidation was employed to convert undoped single-crystal gallium nitride (GaN) into nitrogen-doped polycrystalline β-Ga_2O_3 in the N_2O atmosphere at 1000 °C. A horizontal p-type SBD was fabricated using a "high-magnesium and low-aluminum" alloy (containing 90% Mg and 10% Al by mass) as the circular Schottky contact with a diameter of 2000 μm, directly on the nitrogen-doped β-Ga_2O_3 film without incorporating a p– β-Ga_2O_3 drift layer. At room temperature (300 K), under atmospheric conditions, the SBD exhibited favorable rectification characteristics, with an ideality factor of 1.62. Additionally, the temperature-dependent behavior of the Schottky barrier height and ideality factor was investigated under vacuum conditions.

Keywords: Gallium oxide, Schottky barrier diode, Ideality factor

1. Introduction

Recently, gallium oxide (Ga_2O_3) has gained great attention as a superior candidate of power device to offer an expected outstanding performance beyond the capabilities of the SiC and GaN technologies, as the bandgap (Eg) and the Baliga's figure of merit (FOM) of Ga_2O_3 are much larger than those of SiC and GaN [1–7]. The monoclinic β-Ga_2O_3 is the most stable structure among the five polymorphs of the Ga_2O_3 single crystal, and the vast majority of reported scientific studies have been on the material properties of β-Ga_2O_3.

It is worth commenting on the progress in the processing technological benefits that enable the β-Ga_2O_3 based transistors and diodes may behave as the excellent power devices in real applications. The large-diameter single-crystal of the β-Ga_2O_3 bulks can be economically synthesized by the Czochralski [8], the floating-zone (FZ) [9] and the edge-defined film-fed growth (EFG) [10]. And the high-quality epitaxial growth of β-Ga_2O_3 thin films can be realized via metal-organic chemical vapor deposition (MOCVD) [11], halide vapor phase epitaxy (HVPE) [12], molecular beam epitaxy (MBE) [13], mist chemical vapor deposition (MIST-CVD) [14], pulsed laser deposition (PLD) [15] and plasma-enhanced atomic layer deposition (PEALD) [16]. The n-type doping in β-Ga_2O_3 has been basically realized using the Si [17], Sn [18], Ge [19], Nb [20] shallow donors [21,22]. And the doping concentration can be well controlled in a remarkable wide-range over 10^{14} ~ 10^{20} cm^{-3} [21,22], in the process of the bulk crystals [8], the epitaxial grown [18–22], or by ion-implantation [17]. Based on the successful n-type doping, many promising β-Ga_2O_3 based n-type Schottky barrier diodes (SBD) [23], depletion-mode Metal-Semiconductor Field-Effect Transistors (MESFETs) [24], Metal-Oxide-Semiconductor Field-Effect Transistors (MOSFETs) [25] and even Fin Field-Effect Transistors (FinFETs) [26] have been reported.

In contrast to the current development of the n-type doping, the p-type doping in the β-Ga_2O_3 is still a severe challenge as the acceptor level are deep from the valance band, and the activity energy of the acceptor impurities are high [1–7,27]. Besides, the n-type background in the un-doped β-Ga_2O_3 crystal also produces the self-compensation effect on acceptors, leading to the self-insulation and the native obstacle of the effective p-type conductivity in the material [1–7,27]. Density functional theory (DFT) calculations indicated that nitrogen (N), acting as the substitutional acceptor to oxygen (O), could lead to the p-type conductivity in β-Ga_2O_3 [28]. Successful experiments also reported that by nitrogen-doping [29–30], and the hole mobility was of 41.4 $cm^2/V·s$ [29], and the hole concentration was of 1.64×10^{17} cm^{-3} [30]. Zinc (Zn) was another potential acceptor for provide p-type

conductivity in β-Ga2O3, which was studied by DFT simulation [31,32] and verified by the experiments [27, 31,32]. Based on the Zn-doped β-Ga2O3 nanowire, which was grown on the top of the n-type β-Ga2O3 thin film, a p-n homojunction was fabricated [33]. While, so far the explicit hole concentration had yet been provided by Zn-doping in β-Ga_2O_3. Magnesium (Mg) [32], tungsten (W) [33], selenium (Se) [34], nickel (Ni) [35] and copper (Cu) [36] were also presented as the potential acceptors to produce the p-type conductivity in β-Ga_2O_3. In addition to the above methods of introducing acceptor doped elements as substitutions, as oxygen vacancies play an essential role in effecting the electrical properties of gallium oxide, by heating the β-Ga_2O_3 film in the Co or H_2 atmosphere, the number of oxygen vacancies was reduced, and the p-type conductivity could possibly be fabricated [37]. However, based on the experiments of the above methods, the hole concentration had not obtained as specific and relatively good results as the nitrogen-doped β-Ga_2O_3 [1–7, 27, 29, 30].

In this work, through the thermal oxidation of GaN in N_2O environment at 1000 °C for 60 minutes, the nitrogen-doped p-type β-Ga_2O_3 film with the thickness of 145 nm was successfully achieved. Inspired by the studies that the Zn-doped β-Ga_2O_3 film could also obtain the p-type electrical property [27], Zn was chosen as the ohmic contact to the grown p-type film. Zn electrodes were fabricated by sputtering, followed by the rapid thermal annealing (RTA) at 415 °C for 70 s to form a good ohmic contact. And the 300 K Hall effect measurements under vacuum test environment reported an improved Hall hole concentration of 2.21×10^{18} cm^{-3} cm^{-3}. Then the “high-Mg and low-Al” Schottky contact was grown on the surface of the p-type β-Ga_2O_3 thin film by the laser direct write lithography. Thereafter, the horizontal p-type β-Ga_2O_3 SBD was fabricated.

Without the p– β-Ga_2O_3 drift layer, and without the flattening treatment of film’s surface or the design of the field-plate, this baseline bare SBD was characterized first to extract the fundamental Schottky diode properties using current density–voltage J–V and C–V measurements at room temperature in the atmospheric environment. In the atmospheric environmental test case, the J–V characteristic provided the ideality factor of $n = 1.62$ at room temperature (300 K). After that, to minimize the impact of the adsorption and desorption of gas in the β-Ga_2O_3 film’s porous surface on the conductivity, this p-type β-Ga_2O_3 SBD conducted the J-V and C-V tests under the vacuum environment. In the vacuum test case, the ideality factor n is 1.03 at room-temperature (300 K). Furthermore, the influence of temperature on the interface states of Schottky barrier was investigated by perform the temperature-dependent (from 70 K to 540 K) J-V and C-V tests in vacuum environment.

2. Materials and Methods

The undoped (0001) GaN wafer used in this study was of a native n-type conductivity. To perform the thermal oxidation process, the cleaned GaN wafer was heated in a horizontal quartz tube furnace at a rate of 6.5 $°C\cdot min^{-1}$ to the temperature of 1000 °C, using N_2O gas with a flow rate of 200 $cc\cdot min^{-1}$ for a duration of 60 min. After the oxidation process, the GaN wafer was cooled to room temperature in the N_2O atmosphere. The physical characteristics of the grown nitrogen-doped β-Ga_2O_3 had been reported in [29,30]. And the oxidation thickness measured from the cross-sectional FIB-FESEM image was 145 nm [30]. Further, this work investigated the work-function of the β-Ga_2O_3 film by the ultraviolet photoelectron spectroscopy (UPS). UPS measurement was performed by using a low intensity UV light source (He I line) in an ultra-high vacuum (UHV) apparatus build by SPECS (Berlin, Germany).

In order to form a high-quality ohmic contact to the β-Ga_2O_3 film, the Zn electrodes were prepared by DC-sputtering. The high-purity (≥ 99.999%) Argon (24 sccm) was utilized as the working gas, the background vacuum in the sputtering chamber was maintained below 4.0×10^{-4} Pa, the working pressure during sputtering was set to 0.8 Pa, and the sputtering duration was 20 minutes at a power of 50 W. The zinc electrode was cylindrical, featuring a circular surface with a diameter of 1200 μm and a thickness of 400 nm. As the surface diameter of the zinc electrodes are relatively large, the stainless steel was utilized as a mask layer. Then post-electrode-sputtering, the sample of β-Ga_2O_3 underwent RTA at 415 °C for 70 s in the N_2 environment. The heating and cooling rates were at 100 °C·s−1. Then, the temperature-dependent Rmagnetic-field-dependent Van der Pauw Hall effect measurements were performed (Physical Property Measurement System, PPMS DynaCool-9) to analyze the electrical properties of the β-Ga_2O_3 films in a vacuum environment. Moreover, to fully characterize the microstructures at the Zn to β-Ga_2O_3 interface, the corresponding image at the cross-section of Zn/β-Ga_2O_3 interface was prepared in the form of the lamellae through FIB milling (Helos-5UX), then observed by the selected area electron diffraction SAED and high-resolution transmission electron microscopy (HR-TEM, JEM-F200_TFEG). The elemental mappings were conducted by energy dispersive spectroscopy (EDX).

A 20 nm-thick "high-Mg and low-Al" alloy Schottky electrode was fabricated on the β-Ga_2O_3 film using laser direct-write lithography. To further reduce its resistivity, a 40 nm-thick Au layer was deposited on the alloy. The Schottky electrode features a circular top surface with a diameter of 2000 μm and did not undergo any RTA post-processing. As a result, a lateral Schottky barrier diode with a structure of Zn (anode) / p-type β-Ga_2O_3 / high-Mg low-Al alloy (cathode) was successfully realized.

Then, the DC J-V and AC C-V characteristics of this transverse structure SBD were measured under the atmospheric environmental by the semiconductor parameter analyzer system (Keithley 4200A-SCS, Tektronix Inc., Beaverton, OR, USA). Finally, to gain

inside of the temperature's impact on the Schottky barrier, a temperature-dependent (from 70 K to 540 K) J-V and C-V tests were re-conducted in vacuum environment on a temperature-controlled probe station (Lakeshore PS100) with an Agilent Keysight B1500A parameter analyzer and 4284A Precision LCR Meter.

3. Results

Fig. 1(a) shows the picture of the horizontal structure Zn (anode) / p-type β-Ga_2O_3 / high-Mg low-Al alloy (cathode) SBD. The four electrodes around the 1 × 1 cm square of the β-Ga_2O_3 sample are the Zn ohmic electrodes that underwent a RTA at 415 °C. The larger circular electrode in the center of the β-Ga_2O_3 sample is the Schottky electrode consisting of lower ""high-Mg and low-Al" and upper gold layers without RTA process. Two dashed boxes circle two sets of the transverse SBDs respectively, which are symmetrical and their device characteristics have been tested. The cross-sectional schematic structure and equivalent circuit of the SBD is shown in Fig. 1(b). As it is a p-type SBD, the "high-Mg and low-Al" Schottky electrode is named as cathode, and the Zn ohmic electrode is named as anode.

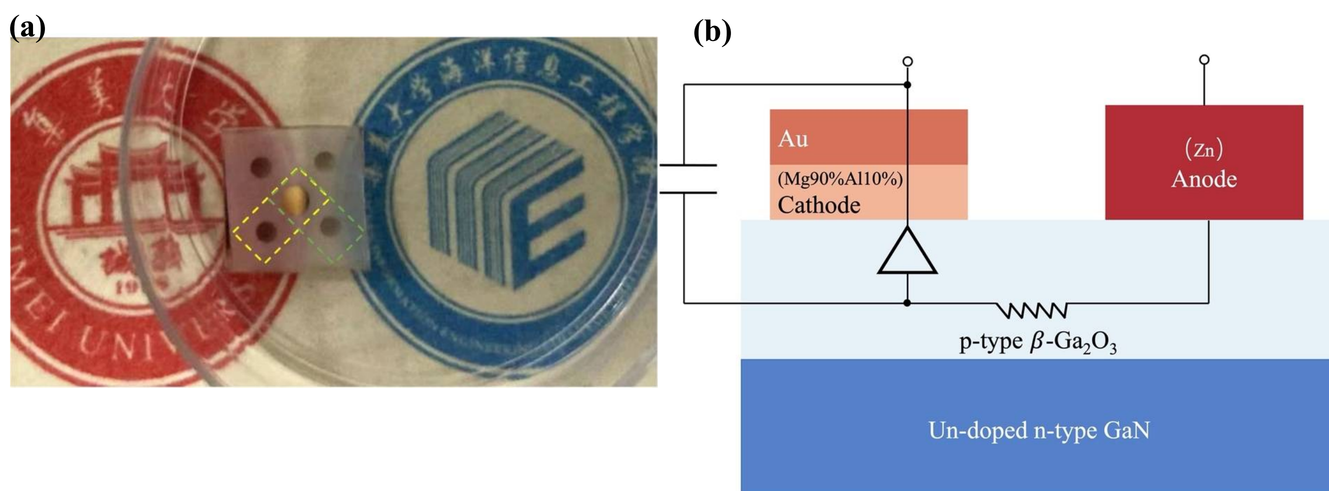

Fig. 1. (**a**) The picture of the horizontal structure p-type β-Ga_2O_3 SBD, (**b**) the cross-sectional schematic structure and equivalent circuit of the p-type β-Ga_2O_3 SBD.

In Table 1, in the vacuum test environment, the temperature-dependent Hall measurements at temperatures of 70 K, 300 K and 400K were carried out for the β-Ga_2O_3 samples with good ohmic contact. The Hall coefficients obtained were all positive, indicating that the β-Ga_2O_3 film was p-type. The f factors are all very close to 1, thus confirming the accuracy of the Hall test.

Table 1. Temperature-dependent (70 K, 300 K, 400 K) Hall effect measurements, in the vacuum test environment, for the β-Ga_2O_3 sample thermally oxidized at 1000 °C.

Parameter	70 K	300 K	400 K
Hall coefficient (carrier type)	23.16	2.83	2.20
f-Factor	0.98	0.99	0.99
Hall hole Concentration (cm^{-3})	2.70×10^{17}	2.21×10^{18}	2.84×10^{18}
Mobility ($cm^2 \cdot V^{-1} \cdot s^{-1}$)	57.53	29.40	15.47
Resistivity (Ω·cm)	0.40	0.10	0.14

The work function of the p-type β-Ga_2O_3 film was directly determined to be 3.99 eV from the UPS measurement as show in Fig. 2. The valence band spectrum (VBM) are determined by extrapolating a linear fit to the leading edge of the spectra to the baseline. And the cut-off energy is calculated to be 17.23 eV. The He lamp used (the laser energy of He I is 21.22 eV), and WS=21.22-17.23=3.99 eV. The work function of β- Ga_2O_3 obtained under thermal oxidation at 1000 °C in an N_2O atmosphere is 3.99 eV.

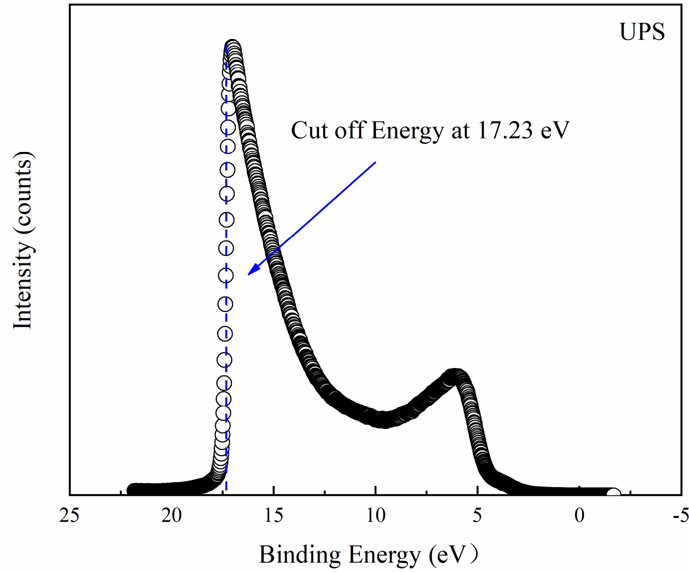

Fig. 2. The UPS photoemission spectra for the p-type β-Ga_2O_3 film. The thresholds of spectra were measured with an extra −5 V bias to achieve a clear cut-off edge.

Fig. 3 illustrates the energy band diagram of the Schottky contact between a p-type semiconductor and a metal. A Schottky barrier readily forms when the work function Ws of the p-type semiconductor exceeds that Wm of the metal. The work functions of Al and Mg are approximately 4.28 eV and 3.66 eV, respectively. From a work function matching standpoint, Mg can form a Schottky contact with the p-type β-Ga_2O_3 film. However, since Mg exists in powder form at high temperatures, fabricating a standalone target material that meets process requirements is highly challenging. To address this issue, after extensive research and repeated experimentation, we adopted an alloying strategy by combining Mg (90 wt%) with Al (10 wt%). This approach yielded a high-Mg, low-Al metal target with a work function of 3.70 eV, which was still lower than the β-Ga_2O_3 sample's work function (3.99 eV), thus satisfying the Schottky contact requirements.

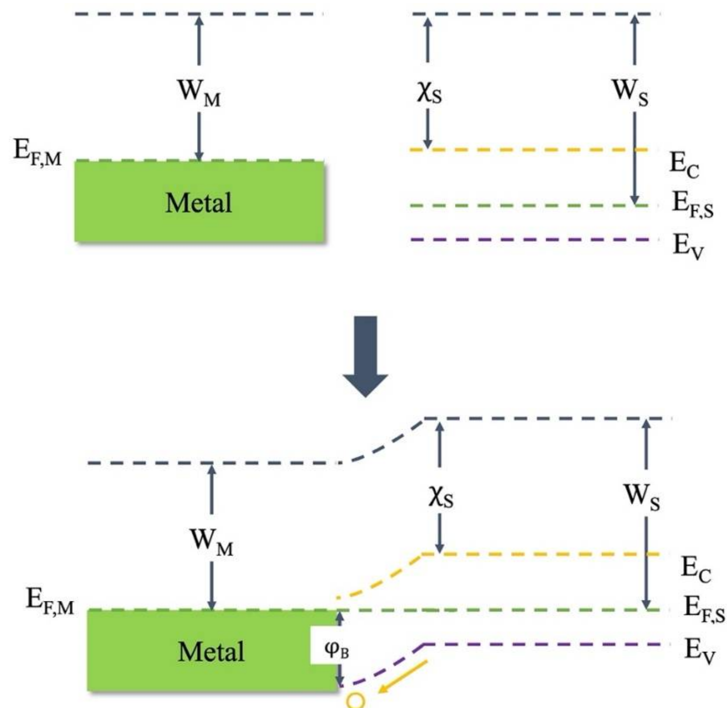

Fig. 3. Energy band diagram of Schottky contact between p-type semiconductor and metal.

Firstly, the I-V and C-V characteristics of the device were tested under atmospheric and room temperature (300 K). The B1500A semiconductor parameter comprehensive test system produced by Keysight Technologies was adopted. A bias voltage ranging from positive 5V to negative 5V was applied to the Schottky diode in the dark environment. The obtained I-V characteristic curve is shown in Fig. 4(a). It is observed that the current is extremely small when negatively biased. However, after switching to positive bias, the current increases rapidly and grows exponentially with the increase of the forward bias voltage, showing a significant rectification effect of the diode, with a rectification ratio of 1.2×10^4. The I-V characteristic curve under forward bias has a linear region. By linear fitting it, the turn-on voltage Von of the Schottky diode is obtained to be 0.32 V. According to the slope of the linear fitting curve, the on-resistance Ron of the Schottky diode is calculated to be $6.6\times10^4\ \Omega$, as shown in Fig. 4(b). The forward I-V characteristic curve of the diode has a linear region in the semi-logarithmic coordinate. The saturation current of the diode is fitted to be 5.6×10^{-9} A, and the ideal factor n is 1.62. According to the calculation from I-V curve, the Schottky barrier height φB is 0.44 eV.

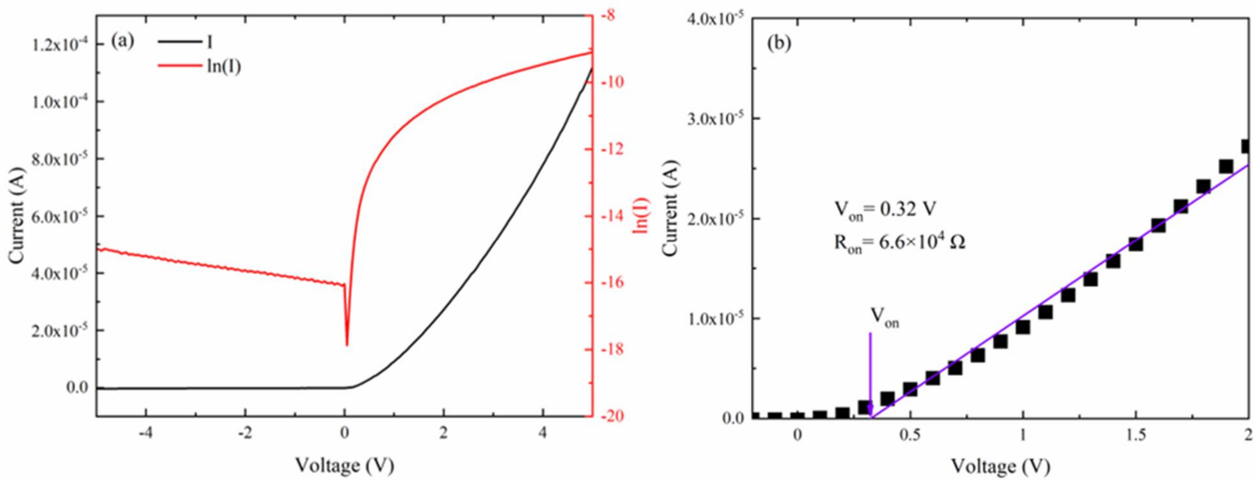

Fig 4. Under atmospheric environment and room temperature (300 K), (**a**) the I-V characteristic curve of the β-Ga_2O_3 Schottky diode (-5 V to +5 V), and (**b**) the forward turn-on voltage Von and on-resistance Ron of the β-Ga_2O_3 Schottky diode.

The C-V test of the device under atmospheric and room temperature (300 K) was carried out, and the test results (1/C2-V) are shown in Fig. 5. And the built-in potential (Vbi) can be calculated by extracting the slope and X-axis intercept of the device 1/C2-V pattern. And Vbi = 0.76 eV.

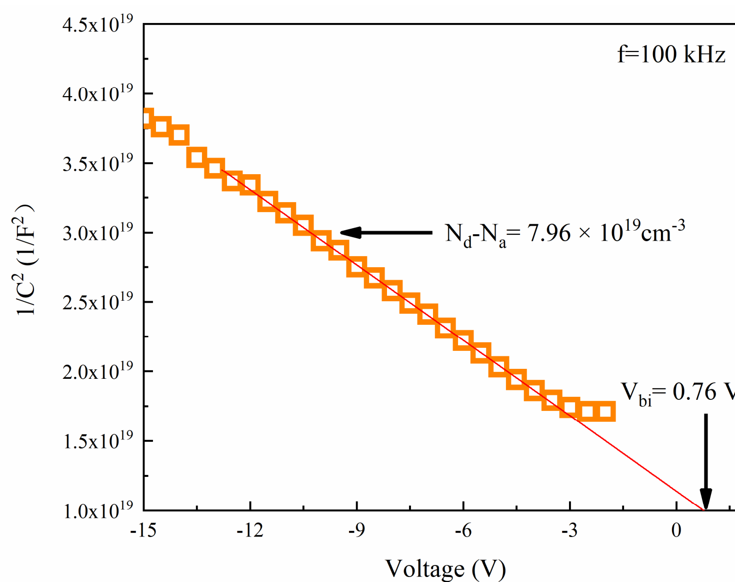

Fig. 5. Under atmospheric environment and room temperature (300 K), the *$1/C^2$-V* characteristic curve of the β-Ga_2O_3 Schottky diode.

It was precisely because no suitable etching method had been found in this study to polish and level the surface of the β-Ga_2O_3 film that the Schottky cross-section would inevitably introduce interface states due to the unevenness of the β-Ga_2O_3 film, thereby affecting the Schottky barrier. Thereafter, the Schottky diode was placed in the vacuum and variable temperature environment for I-V and C-V characteristic testing, with two purposes: (a) the vacuum test environment helped avoid the influence of the water vapor on the device characteristics caused by uneven thin film surfaces. (b) The main operating current of Schottky diodes is the hot electron emission current. And the hot electron emission current and other mechanism currents (such as tunneling current) are all affected by the operating temperature. So the purpose of temperature dependent testing was actually to focus on the effect of temperature on the ideality factor Schottky barrier, and further to focus on the influence of test temperature on the interface states introduced due to surface roughness. Under the vacuum environment, I-V tests were conducted on the samples at six temperature gradients ranging from 150 K to 400 K (specifically 150 K, 200 K, 250 K, 300 K, 350 K and 400 K). And the current-density-voltage (J-V) and ln(J)-V characteristic curves were plotted accordingly in Fig. 6(a) and (b). In Fig. 6(a), the J-V characteristics of the Schottky diode showed a clear changing trend. As the temperature rises, the threshold voltage of the device gradually decreases, and the growth rate of the current density accelerates. This phenomenon is attributed to the fact that high temperature promotes the excitation of majority carriers, increases the carrier concentration at the interface, and reduces the width of the depletion region of the potential barrier, thereby facilitating the carrier crossing the potential barrier. The curve graphs of J-V voltage were plotted in the semi-logarithmic coordinate system, as shown in Fig. 6 (b). After linear fitting of the linear part, the slope of the line is used to calculate the ideal factor n of the Schottky barrier diode, while the y-intercept of the line is used to calculate the height φB of the Schottky barrier.

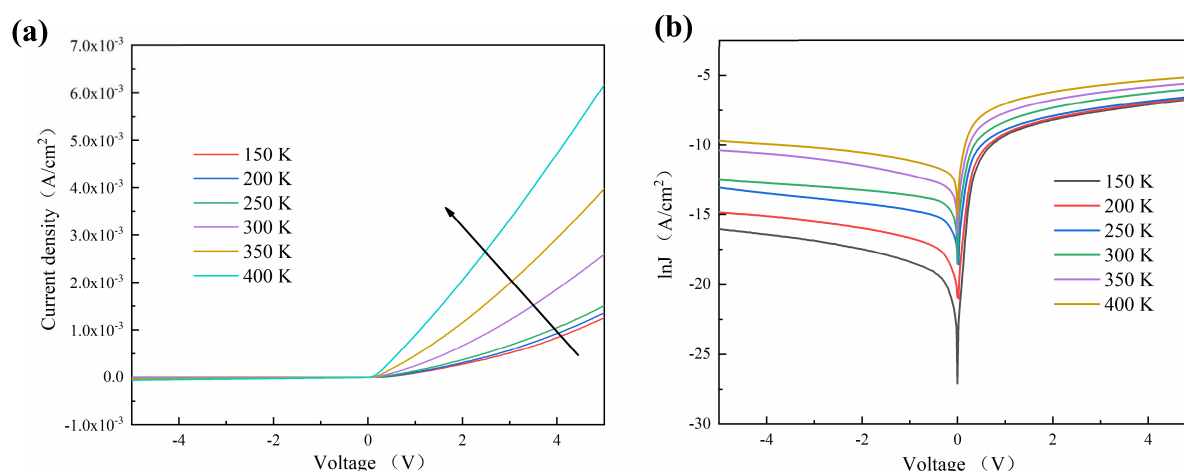

Fig. 6. In a vacuum environment, at the temperature range of 150 K, 200 K, 250 K, 300 K, 350 K and 400 K, (**a**) the forward *J–V* characteristics, and (**b**) *ln(J)-V* characteristics.

In a vacuum environment, the calculated ideal factor and Schottky barrier height as functions of temperature are presented in Fig. 7 and Table 2. As the temperature increased, the ideal factor exhibited a gradual decreasing trend, with values particularly close to 1 in the 300-400 K range. Concurrently, the Schottky barrier height increased with rising temperature. This phenomenon occurred because carrier transport across the potential barrier was a temperature-dependent process. At lower test temperatures, carriers primarily relied on quantum tunneling to overcome the higher potential barrier. Consequently, in addition to thermionic emission current, tunneling current contributed significantly to carrier transport, resulting in an ideal factor n substantially greater than 1. As the temperature increased, more carriers gained sufficient energy to surmount the potential barrier through thermal excitation. This reduced the relative contribution of tunneling current while increasing the proportion of thermionic emission current, causing the ideal factor to gradually approach unity.

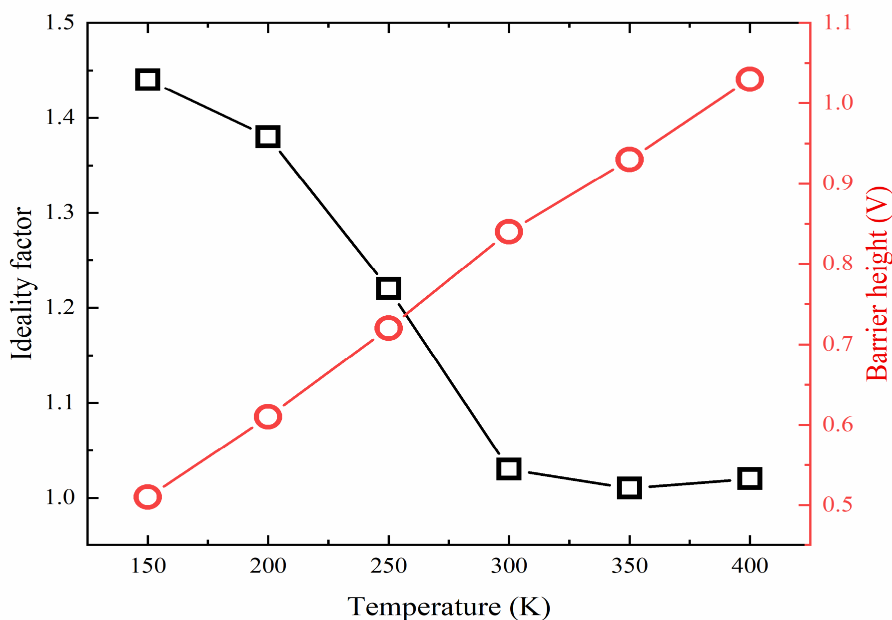

Fig. 7. In a vacuum environment, the trend graph of the ideal factor and barrier height varying with the test temperature in a vacuum environment at a temperature of 150-400 K.

Table 2. Temperature-dependent (150-400 K) ideality factors and the Schottky barrier heights, in the vacuum test environment.

Test temperature (K)	Ideality factor n	Schottky barrier height (eV)
150	1.44	0.51
200	1.38	0.61
250	1.22	0.72
300	1.03	0.84
350	1.01	0.93
400	1.02	1.27

In summary, due to the surface inhomogeneity of the β-Ga_2O_3 film, the Schottky contact exhibited non-uniform characteristics, resulting in spatially inconsistent barrier heights at the metal-semiconductor interface. The vacuum and variable-temperature test results further demonstrated that this Schottky contact non-uniformity indeed, to a considerable extent, influenced the device's electrical performance as temperature varied..

4. Conclusions

In this study, we fabricated Schottky barrier diodes using p-type β-Ga_2O_3. The devices exhibited clear rectifying characteristics during room-temperature I-V and C-V measurements in ambient atmosphere, demonstrating an on-off current ratio of 1.2×10^4, a turn-on voltage of 0.32 V, an on-resistance of 6.6×10^4 Ω, and an ideality factor (n) of 1.62. The current-voltage characteristics yielded a barrier height (φB) of 0.44 eV. Variable-temperature I-V measurements conducted under vacuum revealed temperature-dependent characteristics: the ideality factor decreased from 1.44 (150 K) to 1.02 (400 K), while the barrier height increased from 0.51 eV (150 K) to 1.27 eV (400 K). Our analysis suggested that these variations originated from the inhomogeneous Schottky contact caused by surface roughness of the β-Ga_2O_3 film. The considerable barrier height non-uniformity, combined with temperature-sensitive interface states at the non-uniform contact, ultimately led to the strong temperature dependence of the ideality factor. Therefore, the current Schottky barrier diode represents a prototype device. Future research should focus on developing effective gallium oxide film planarization techniques to minimize interface states induced by surface roughness at Schottky contacts.

Author Contributions: H. Zhou carried out the experiments, X. Wang and W. Chen analyzed the data and measurements, S. Wei designed the experimental and test schemes, organized the data, and wrote the paper.

Funding: This research was funded by the post-subsidy project for industry education research of Xiamen Science and Technology Bureau, Fujian Province, China (Grant No. 2023CXY0322).

Data Availability Statement: The data of this study are available from the corresponding author upon reasonable request.

Conflicts of Interest: The authors declare no conflict of interest.

References

1. Pearton, S.J.; Yang, J.; Cary, P.H.; Ren, F.; Kim, J.; Tadjer, M.J.; et al. A review of Ga_2O_3 materials, processing, and devices. Appl. Phys. Rev. **2018**, *5*, 011301. https://doi.org/10.1063/1.5006941
2. Higashiwaki, M.; Sasaki, K.; Murakami, H.; Kumagai, Y.; Koukitu, A.; Kuramata, A.; et al. Recent progress in Ga_2O_3 power devices. Semicond. Sci. Technol. **2016**, *31*, 034001. https://doi.org/10.1088/0268-1242/31/3/034001.
3. Mastro, M.A.; Kuramata, A.; Calkins, J.; Kim, J.; Ren, F.; Pearton, S.J. Perspective-Opportunities and Future Directions for Ga_2O_3. ECS J. Solid State Sci. Technol. **2017**, *6*, P356–P359. https://doi.org/10.1149/2.0031707jss.
4. Galazka, Z. β-Ga_2O_3 for wide-bandgap electronics and optoelectronics. Semicond. Sci. Technol. **2018**, *33*, 113001. https://doi.org/10.1088/1361-6641/aadf78.
5. Tsao, J.Y.; Chowdhury, S.; Hollis, M.A.; Jena, D.; Johnson, N.M.; Jones, K.A.; et al. Ultrawide-Bandgap Semiconductors: Research Opportunities and Challenges. Adv. Electron. Mater. **2018**, *4*, 1600501. https://doi.org/10.1002/aelm.201600501.
6. Xue, H.; He, Q.; Jian, G.; Long, S.; Pang, T.; Liu, M. An Overview of the Ultrawide Bandgap Ga_2O_3 Semiconductor-Based Schottky Barrier Diode for Power Electronics Application. Nanoscale Res. Lett. **2018**, *13*, 290. https://doi.org/10.1186/s11671-018-2712-1.
7. Higashiwaki, M.; Kuramata, A.; Murakami, H.; Kumagai, Y. State-of-the-art technologies of gallium oxide power devices. J. Phys. D Appl. Phys. **2017**, *50*, 333002. https://doi.org/10.1088/1361-6463/aa7aff
8. Galazka, Z.; Irmscher, K.; Uecker, R.; Bertram, R.; Pietsch, M.; Kwasniewski, A.; et al. On the bulk β-Ga_2O_3 single crystals grown by the Czochralski method. J. Cryst. Growth **2014**, *404*, 184–191. https://doi.org/10.1016/j.jcrysgro.2014.07.021
9. Suzuki, N.; Ohira, S.; Tanaka, M.; Sugawara, T.; Nakajima, K.; Shishido, T. Fabrication and characterization of transparent conductive Sn-doped β-Ga_2O_3 single crystal. Phys. Status Solidi C **2007**, *4*, 2310–2313. https://doi.org/10.1002/pssc.200674884
10. Mu, W.; Jia, Z.; Yin, Y.; Hu, Q.; Li, Y.; Wu, B.; et al. High quality crystal growth and anisotropic physical characterization of β-Ga_2O_3 single crystals grown by EFG method. J. Alloys Compd. **2017**, *714*, 453–458. https://doi.org/10.1016/j.jallcom.2017.04.185
11. Feng, Z.; Bhuiyan, A.F.M.A.U.; Kalarickal, N.K.; Rajan, S.; Zhao, H. Mg acceptor doping in MOCVD (010) β-Ga_2O_3. Appl. Phys. Lett. **2020**, *117*, 222106. https://doi.org/10.1063/5.0031562
12. Modak, S.; Lundh, J.S.; Al-Mamun, N.S.; Chernyak, L.; Haque, A.; Tu, T.Q.; et al. Growth and characterization of α-Ga_2O_3 on sapphire and nanocrystalline β-Ga_2O_3 on diamond substrates by halide vapor phase epitaxy. J. Vac. Sci. Technol. A **2022**, *40*, 062703. https://doi.org/10.1116/6.0002115
13. Kalarickal, N.K.; Xia, Z.; McGlone, J.; Krishnamoorthy, S.; Moore, W.; Brenner, M.; et al. Mechanism of Si doping in plasma assisted MBE growth of β-$Ga_2O_3O_3$. Appl. Phys. Lett. **2019**, *115*, 152106. https://doi.org/10.1063/1.5123149.
14. Mondal, A.K.; Deivasigamani, R.; Ping, L.K.; Shazni Mohammad Haniff, M.A.; Goh, B.T.; Horng, R.H.; et al. Heteroepitaxial Growth of an Ultrathin β-Ga_2O_3 Film on a Sapphire Substrate Using Mist CVD with Fluid Flow Modeling. ACS Omega **2022**, *7*, 41236–41245. https://doi.org/10.1021/acsomega.2c04888.
15. Wakabayashi, R.; Oshima, T.; Hattori, M.; Sasaki, K.; Masui, T.; Kuramata, A.; et al. Oxygen-radical-assisted pulsed-laser deposition of β-Ga_2O_3 and β-$(AlxGa1-x)_2O_3$ films. J. Cryst. Growth **2015**, *424*, 77–79. https://doi.org/10.1016/j.jcrysgro.2015.05.005.
16. Fan, H.-C.; Wang, C.; Ruan, Y.-J.; Shen, K.-C.; Wu, W.-Y.; Wuu, D.-S.; et al. Enhanced Responsivity of Solar Blind Ultraviolet Photodetector by PEALD Deposited Zn-Doped Ga_2O_3 Thin Films. IEEE Trans. Electron Devices **2024**, *71*, 664–669. https://doi.org/10.1109/TED.2023.3336853.
17. Tarntair, F.; Huang, C.; Rana, S.; Lin, K.; Hsu, S.; Kao, Y.; et al. Material Properties of n-Type β-Ga_2O_3 Epilayers with In Situ Doping Grown on Sapphire by Metalorganic Chemical Vapor Deposition. Adv. Electron. Mater. **2024**, 2300679. https://doi.org/10.1002/aelm.202300679.
18. Seo, D.; Baek, J.; Kim, S.; Cho, B.J.; Hwang, W.S. Sn-doped n-type amorphous gallium oxide semiconductor with energy bandgap of 4.9 eV. Mater. Sci. Semicond. Process. **2024**, *169*, 107922. https://doi.org/10.1016/j.mssp.2023.107922.
19. Han, S.-H.; Mauze, A.; Ahmadi, E.; Mates, T.; Oshima, Y.; Speck, J.S. n-type dopants in (001) β-Ga_2O_3 grown on (001) β-Ga_2O_3 substrates by plasma-assisted molecular beam epitaxy. Semicond. Sci. Technol. **2018**, *33*, 045001. https://doi.org/10.1088/1361-6641/aaae56
20. Zhou, W.; Xia, C.; Sai, Q.; Zhang, H. Controlling n-type conductivity of β-Ga_2O_3 by Nb doping. Appl. Phys. Lett. **2017**, *111*, 242103. https://doi.org/10.1063/1.4994263.
21. Varley, J.B.; Weber, J.R.; Janotti, A.; Van de Walle, C.G. Oxygen vacancies and donor impurities in β-Ga_2O_3. Appl. Phys. Lett. **2010**, *97*, 142106. https://doi.org/10.1063/1.3499306.

22. Chou, T.-S.; Bin Anooz, S.; Grüneberg, R.; Irmscher, K.; Dropka, N.; Rehm, J.; et al. Toward Precise n-Type Doping Control in MOVPE-Grown β-Ga_2O_3 Thin Films by Deep-Learning Approach. Crystals **2021**, *12*, 8. https://doi.org/10.3390/cryst12010008.
23. Qin, Y.; Xiao, M.; Porter, M.; Ma, Y.; Spencer, J.; Du, Z.; et al. 10-kV Ga_2O_3 Charge-Balance Schottky Rectifier Operational at 200 °C. IEEE Electron Device Lett. **2023**, *44*, 1268–1271. https://doi.org/10.1109/LED.2023.3287887.
24. Bae, J.; Kim, H.W.; Kang, I.H.; Yang, G.; Kim, J. High breakdown voltage quasi-two-dimensional β-Ga_2O_3 field-effect transistors with a boron nitride field plate. Appl. Phys. Lett. **2018**, *112*, 122102. https://doi.org/10.1063/1.5018238.
25. Goyal, P.; Kaur, H. Exploring the efficacy of implementing field plate design with air gap on β-Ga_2O_3 MOSFET for high power & RF applications. Micro Nanostructures **2023**, *173*, 207454. https://doi.org/10.1016/j.micrna.2022.207454.
26. Xu, S.; Liu, L.; Qu, G.; Zhang, X.; Jia, C.; Wu, S.; et al. Single β-Ga_2O_3 nanowire based lateral FinFET on Si. Appl. Phys. Lett. **2022**, *120*, 153501. https://doi.org/10.1063/5.0086909.
27. Shanshan, R.; Ma, J.; He, Z.; Xiaoqian, F. The effort of finding p-type β-Ga_2O_3-a review of theoretical and experimental research. In *Seventh Symp. Nov. Photoelectron. Detect. Technol. Appl.*; Chu, J., Yu, Q., Jiang, H., Su, J., Eds.; SPIE: Kunming, China, **2021**; p. 85. https://doi.org/10.1117/12.2586313.
28. Ma, C.; Wu, Z.; Jiang, Z.; Chen, Y.; Ruan, W.; Zhang, H.; et al. Exploring the feasibility and conduction mechanisms of P-type nitrogen-doped β-Ga_2O_3 with high hole mobility. J. Mater. Chem. C **2022**, *10*, 6673–6681. https://doi.org/10.1039/D1TC05324H.
29. Liu, Y.; Wei, S.; Shan, C.; Zhao, M.; Lien, S.-Y.; Lee, M. Compositions and properties of high-conductivity nitrogen-doped p-type β-Ga_2O_3 films prepared by the thermal oxidation of GaN in N2O ambient. J. Mater. Res. Technol. **2022**, *21*, 3113–3128. https://doi.org/10.1016/j.jmrt.2022.10.110.
30. Wei, S.; Liu, Y.; Shi, Q.; He, T.; Shi, F.; Lee, M. Further Characterization of the Polycrystalline p-Type β-Ga_2O_3 Films Grown through the Thermal Oxidation of GaN at 1000 to 1100 °C in a N2O Atmosphere. Coatings **2023**, *13*, 1509. https://doi.org/10.3390/coatings13091509.
31. Kaneko, K.; Fujita, S. Novel p-type oxides with corundum structure for gallium oxide electronics. J. Mater. Res. **2022**, *37*, 651–659. https://doi.org/10.1557/s43578-021-00439-4.
32. Islam, M.M.; Liedke, M.O.; Winarski, D.; Butterling, M.; Wagner, A.; Hosemann, P.; et al. Chemical manipulation of hydrogen induced high p-type and n-type conductivity in Ga_2O_3. Sci. Rep. **2020**, *10*, 6134. https://doi.org/10.1038/s41598-020-62948-2.
33. Dakhel, A.A. Structural, optical, and opto-dielectric properties of W-doped Ga_2O_3 thin films. J. Mater. Sci. **2012**, *47*, 3034–3039. https://doi.org/10.1007/s10853-011-6134-z.
34. Bai, R.; Zhao, B.; Ling, K.; Li, K.; Liu, X. Dilute-selenium alloying: A possible perspective for achieving p-type conductivity of β-gallium oxide. J. Alloys Compd. **2022**, *891*, 161969. https://doi.org/10.1016/j.jallcom.2021.161969.
35. Hwang, T.-Y.; Choi, Y.; Song, Y.; Eom, N.S.A.; Kim, S.; Cho, H.-B.; et al. A noble gas sensor platform: linear dense assemblies of single-walled carbon nanotubes (LACNTs) in a multi-layered ceramic/metal electrode system (MLES). J. Mater. Chem. C **2018**, *6*, 972–979. https://doi.org/10.1039/C7TC03576D.
36. Zhang, C.; Li, Z.; Wang, W. Critical Thermodynamic Conditions for the Formation of p-Type β-Ga_2O_3 with Cu Doping. Materials **2021**, *14*, 5161. https://doi.org/10.3390/ma14185161.
37. Deng, Z.-Y.; Kumar, U.; Ke, C.-H.; Lin, C.-W.; Huang, W.-M.; Wu, C.-H. A simple and fast method for the fabrication of p-type β-Ga_2O_3 by electrochemical oxidation method with DFT interpretation. Nanotechnology **2023**, *34*, 075704. https://doi.org/10.1088/1361-6528/aca2b1

Publisher's Note: IIKII stays neutral with regard to jurisdictional claims in published maps and institutional affiliations.

© 2026 The Author(s). Published with license by IIKII, Taiwan. This is an Open Access article distributed under the terms of the Creative Commons Attribution License (CC BY), which permits unrestricted use, distribution, and reproduction in any medium, provided the original author and source are credited.